RC23024 (W0312-037) December 9, 2003
Physics

IBM Research Report

Domain Walls, Bloch-Line Vortices, and Their Resonances Imaged in Garnet Films Using Cotton-Mouton Magneto-Optics

Bernell E. Argyle
IBM Research Division
Thomas J. Watson Research Center
P.O. Box 218
Yorktown Heights, NY 10598

Research Division
Almaden - Austin - Beijing - Haifa - India - T. J. Watson - Tokyo - Zurich

DOMAIN WALLS, BLOCH-LINE VORTICES, AND THEIR RESONANCES IMAGED IN GARNET FILMS USING COTTON-MOUTON MAGNETO-OPTICS

BERNELL E. ARGYLE
IBM Thomas J Watson Research Center
Yorktown Heights, NY 10598

Abstract: Microscopic images of domain walls, Bloch-lines, magnetic vortices, and their resonances in iron-garnet films are formed using the magneto-optical Cotton-Mouton effect (CM). Results reported in 1984 which were the first to image Bloch-lines optically, are summarized. In our sample epitaxial garnet film of $Eu_{0.7}Tm_{0.5}Ga_{0.85}$:YIG, the domain moments lie in the [100] film plane. A pattern created with ion irradiation stabilizes the in-plane domains along four-fold "easy axes" [110]. CM microphotographs of 180^0 Neél walls show that multiple Bloch-line vortices may be present. A single vortex occurs at the intersection of two 90^0 Neél walls. For two 90^0 walls intersecting orthogonally, the motions observed at resonance induced with in-plane rf fields reveal the vortex motion is *circular*. The frequency of resonance depends on the length of the intersecting walls. Resonances appear at 24, 15.5 and 13 MHz for wall lengths 14, 28 and 35 μm respectively. Slonczewski estimated theoretically that the contribution of the effective areal mass of the 90^0 walls to the resonance frequency is negligible. His model resonances based on restoring forces arising from stray field energy when walls displace from equilibrium, are found in reasonable agreement with the experiment. The circular motion at resonance essentially involves precessions of just those electron spins within the invisibly small vortex-core region, and it confirms experimentally the existence of a Magnus force orthogonal to the velocity of a simple quantized magnetic vortex. The vortex core in our film carries magnetic film-normal flux equal 3% of a flux quantum, ch/2e. Very recently, Park, *et al* [Phys. Rev. B, vol. **77**, 020403(R)] formed MFM images of single vortices isolated in Permalloy nano particles and measured their time-resolved impulse response. We briefly compare the magneto dynamics they observed with our observations in the garnet film when the vortex is part of a wall network.

Key words: Garnet, magneto-optic imaging, domain walls, Bloch lines, magnetic vortices, vortex resonance, Magnus force, Cotton-Mouton

1. BACKGROUND

The observation of domains and domain walls using magneto-optical microscopy has been of considerable importance for nearly four decades, both technically and fundamentally. In the decade of the 1970s epitaxial iron-garnet films where investigated for magnetic memory applications. Their composition and magnetic properties were arranged so that the domain moments pointed *perpendicular* to the film plane. Although not directly observable optically, localized reversals or 'twists' in magnetization can occur within the domain wall. These 'twists' called Bloch lines, were first made visible with the Bitter solution method [1]. The BLs have considerable influence on observable dynamic displacements of 'bubble' domains [2]. More recently, garnet films have been found useful as magneto-optical 'indicators' of localized fields whereby field induced changes in magnetization are readily detected using the Faraday effect [3]. The favored type of film for this application is a planar anisotropy film in which the remnant domain moments lie largely *in plane*. However, the possible influences of Bloch lines (or vortices within Bloch lines) on their magneto dynamic response, has received little attention.

In 1984 we demonstrated [4] that Bloch lines in Neél walls of garnet films can be imaged magneto-optically even when the wall moment lies in the film plane and its scale falls below the limit of optical resolution. Here, we review how the image itself and a continuity argument together with measurements of domain-wall frequency response [5], showed us that Bloch-lines in Neél walls contain *magnetic vortices* which exhibit unique properties. We summarize our seminal method of imaging Bloch-line vortices using the magneto-optical Cotton-Mouton effect. Swept frequency measurements made with our apparatus described in [6] have also revealed the fundamental influence which magnetic vortices have on the motions of a Neél-wall network.

Very recently, isolated magnetic vortices were investigated in Permalloy 'nanodots' [7] using modern methods having higher spatial and temporal resolutions.

2. EXPERIMENTAL

A 0.79 μm thick $Eu_{0.7}Tm_{0.5}Ga_{0.85}$:YIG film was epitaxially grown on a (100) $Gd_3Ga_5O_{12}$ substrate. The film's parameters are: growth anisotropy, $K_u = -4x10^4$ erg/cm^3, gyromagnetic ratio $\gamma = 1.37x10^7$ s^{-1}Oe^{-1}, $4\pi M = 350$G, crystal anisotropy $K_1 = -7x10^3$ erg/cm^3, and exchange parameter $A = 2x10^{-7}$ erg/cm. The large negative K_u forces the magnetization into the film plane. The small negative K_1 produces 'easy' axes parallel to the four-fold in-plane [110].

Domain networks in films exhibit configurational instability. So, we stabilize a simple network by fixing walls at their ends. This is accomplished by masking and implanting with He^{+2} having energies (80 and 240 KeV) and flux ($3x10^7$ cm^{-2}) sufficient to produce $M = 0$ in unmasked regions. Boundaries made parallel to [110] stabilize domains along [110] 'easy' axes, making adjacent domains antiparallel- or orthogonal to each other, as illustrated in Fig. 1a.

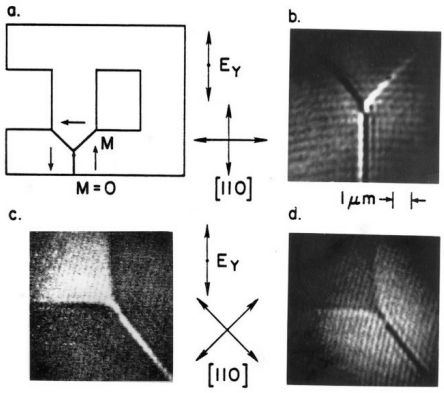

Fig. 1. Bloch-line and Neél walls between [110] easy-axis domains in (100) garnet film. Structure (a) stabilizes wall pattern for magnetic birefringence images in (b)-(d). (adapted from Ref. 5).

3. COTTON-MOUTON CONTRAST and MAGNETIC STRUCTURES

The Cotton-Mouton effect is due to magnetic linear birefringence (MLB) in contrast to circular birefringence for the Faraday effect. MLB causes an optical phase difference of transmitted polarized light due to a difference in refractive indices for polarizations parallel and perpendicular, to ***M***. So, polarization of light on the far side of a film is elliptical in the general case when incident polarization is neither parallel nor perpendicular to ***M***. In order to produce CM contrast, the polarizing microscope requires normally incident light with crossed polarizers and an adjustable optical phase compensator. Images presented [Figs. 1(b-d) and 4a] were obtained with an oil-immersion 100x 1.3NA objective and 488 nm laser illumination. Domain ***M***-alignments (Fig. 1a) were checked with our instrument described in Ref. 6 using Faraday contrast under oblique illumination. Curved striations in the background are an artifact due to the laser coherence and interference in the faceplate of a SIT television camera. The artifact is not associated with the sample or microscope optics. It does not appear in binocular view.

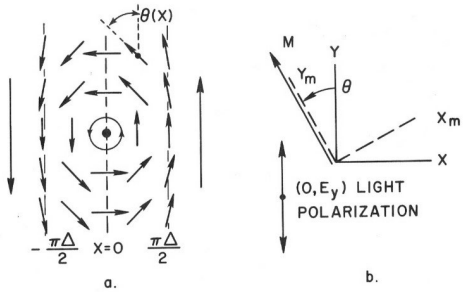

Fig. 2. (a) Continuous rotation model of 180^0 wall near a Bloch-line vortex; (b) Reference frames x-y of laboratory and x_m - y_m rotated according to the magnetic vector ***M***. (adapted from Ref. 5)

The structure of a 180° Neél wall (Fig. 2a) is a continuous rotation $\theta = \pm\arctan[\exp(x/\Delta)]$ of local magnetization with distance x from the wall center, where $\Delta = (A/2\pi M^2)^{1/2}$ is the wall-width parameter. Small effects of crystal anisotropy K_1 are neglected. This continuous model is illustrated in Fig. 2a. We may also adopt a linear structure, $\theta = \pm[(\pi x/W)-\pi/2]$, in the range $(-W/2 \leq x \leq W/2)$ where $W=\pi 2^{1/2}\Delta$ [1]. This simpler linear model is illustrated in Fig. 3(a) for regions above and below the Bloch line.

To explain CM contrast one considers two eigenmodes of propagating light having electric vector components parallel and perpendicular to the local magnetization ***M***. Thus, we transform the incident polarized light components (E_x, E_y) referred to the laboratory frame, into components (E_{xm}, E_{ym}) referred to the frame of ***M*** (Fig. 2b) rotated by θ(x) about the film normal according to the wall model. The CM magnetic linear birefringence (MLB) is invoked in the frame of ***M*** to obtain the state of polarized transmitted light E' where it produces a phase difference $\delta\psi=(\psi_{\rightleftarrows}-\psi_{\text{ff}})$ arising at the far side of the film from the difference in velocity for the two eigenmodes.

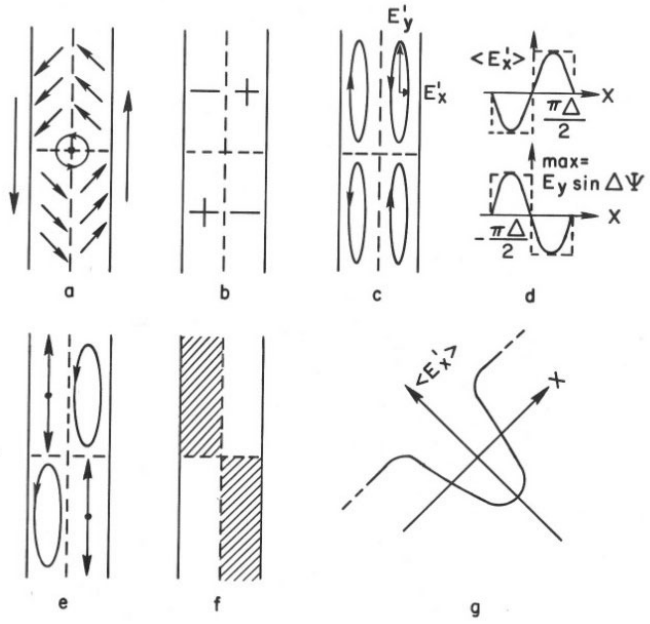

Fig. 3. Diagrams for model explaining magneto-optic patterns in vortex region of Fig. 1. (adapted from Ref. 5)

For incident light E_y polarized along y as in Figs.1-3, the transmitted light is approximately

$$\mathbf{E'} \cong E_y e^{i\overline{\psi}} (\sin 2\theta \cdot \delta\Psi\hat{x} + \hat{y}) \qquad (1)$$

where $\delta\psi = (\psi_\perp - \psi_{||})/2 = 2\pi h(n_\perp - n_{||})/\lambda_0$ and $\overline{\psi} = (\psi_\perp + \psi_{||})/2$ [4]. The factor $\sin 2\theta$ reflects the *quadratic* effect with $\boldsymbol{M}$. The presence of $e^{i\pi/2}$ gives the 90^0 phase shift between the two components, making the light elliptically polarized. Whether it is right- or left handed depends on sign of the prefactor, $\sin 2\theta \cdot \delta\psi$. Assuming $\delta\psi > 0$, the arrangement of spins shown in Fig. 3a, yields the signs shown in Fig. 3b which in turn causes the elliptical polarizations in Fig. 3c. The degree of ellipticity E'_x/E'_y depends on the amplitude E'_x plotted in Fig. 3d and fixed amplitude $E'_y \cong E_y$ (not shown). The maximum amplitude E'_x attributable to the factor $E_y\,\delta\psi$ is small compared with E'_y because our 0.8μm garnet film is thin compared to the absorption length ($\alpha^{-1} \approx 0.5\mu m$) and because MLB from the CM effect is weak, measured here as $\delta\psi \approx 10^{-4}$ rad. The solid line in Fig. 3d derives from the Neél wall-rotation model, inserted in Eq. (1). The dashed line is for the conveniently simple sub-domain-wall model (Fig. 3a) in which M_{wall} has the discrete orientations $\theta_l = (2l+1)\pi/4$ *(l = integer)* accorded to the l_{th}-quadrant (Fig. 3a).

That CM contrast is *quadratic* in- and directly sensitive to *planar* components M_{xy} makes it ideal for magneto-optic imaging *planar* anisotropy films and for revealing signs of twist in magnetization of Neél-wall segments and positions of Bloch lines. To make maximum contrast, either (but not both) senses of elliptical light (Fig. 3c) are converted to linear light by inserting the adjustable compensator with its biaxis at 45^0 with respect to principle axes (x,y) of the ellipse. Elliptical light of one sense is converted to linear light by adjusting the compensator; light of the opposite sense becomes correspondingly more circular (Fig.3e). Finally, the optical analyzer set to extinguish E'_y produces the black/white 180^0 wall contrast depicted in Fig. 3f, which is consistent with the photograph in Fig. 1b.

We can apply this model to the case when the film was rotated by 45° [Fig. 1(c,d)]. Replacing θ by $\theta+45^0$ in Eq. (1) yields the curve for E'_x shown in Fig. 3g. This indeed produces a dark wall contrasting against two adjacent bright 180^0 domains. This explains the photography of Fig. 1d. Inverse contrast (Fig. 1c) occurs when the sign of the optical compensator is reversed.

Domain contrast is also observed in the case of the 45° rotated film (Fig. 1c,d), but only between domains differing by 90°. This is because elliptical polarization is again induced by the MLB in any domain not oriented precisely along a principal axis established by the incident polarization. These contrast effects further certify the quadratic dependence on the magnetic vector $\boldsymbol{M}$ of the magneto-optic effect responsible for the wall contrast.

A quadratic MLB effect may have two origins: the ordinary Cotton-Mouton effect associated with exchange splitting of excited states [9], and the Pockels piezo-optic effect which can arise from magneto-elastic deformations [10]. The latter is negligible in our film for two reasons. For pure YIG crystals Dedukh and Nikitenko showed with their measurements of piezo-optic and magnetostriction coefficients, that magnetostrictive deformations would contribute less than one percent of the total MLB [10]. Also, an analysis like that of Kryder, *et al* [1] including effects of film deformations decaying into the substrate, shows that the contribution to the wall energy density from magnetoelastic effects in our garnet film is less than 1% of the total.

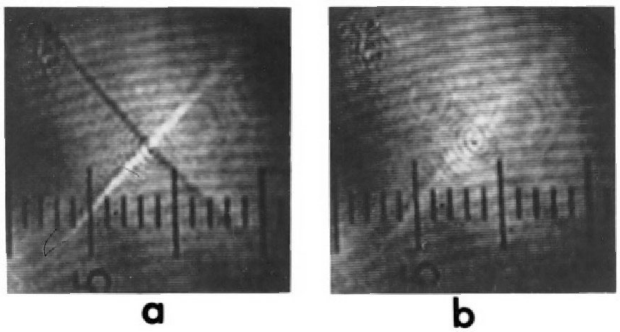

Fig. 4. Photographs of intersecting 90^0 walls in (a) static and (b) excited resonant oscillation. (See text.) The scale is one micron per division. (adapted from Ref. 5)

4. VORTEX STRUCTURE AND DYNAMIC RESPONSE

Figure 5(a) gives the CM contrast image of two 90^o walls crossing each other orthogonally. The applied field is zero. All four wall ends are fixed at inside corners of a 'Swiss cross' pattern [Ref. 5. Fig. 1a]. Outside the pattern M=0 was produced by ion irradiation. This structure allowed making the first direct observation of resonant motion of a magnetic vortex. Attempts proved less successful using the vortex in the wall network of Fig. 1, because walls of that structure did not have of a well-defined restoring force due a small permeable closure domain (not shown) at the end of the 180^0 wall. A wall's contrast in Fig. 4a depends on its ***M***-orientation and the sign of the retardation due to the optical compensator. The bright Neél walls have ***M*** at $\theta = 45^0$ and 225^0 with respect to the incident light ($0, E_y$) while the dark walls are at 135^0 and 315^0 . The intersection of the two 90° Neél walls is a magnetic vortex as illustrated schematically in Ref. 5, Fig. 1(b). Fixing the four ends of the walls to the inner corners, immobilizes wall ends and defines the wall's restoring force. Moreover, the walls do not touch closure domains, making this configuration most suitable for conclusive comparison of experiment with theory.

Although too small to be resolved, the center of the wall junction, - by continuity -, must have vortex structure of a type well known theoretically [11] but not previously seen directly. Consider a circuit centered at the junction. If the radius R is large compared both to optical resolution and thickness of the wall $\Delta = 2^{-1}\pi(A/K_1)^{1/2} \approx 0.1\mu m$, the microscope contrast reveals a pattern of magnetic vectors whose angle increases by 2π. On a circle with $R < \Delta$, θ must also increase by 2π by continuity. In addition, theoretically [11], the spins deviate from the xy film plane within a radius $(A/K_u)^{1/2}$ of the vortex core, which in our case, is about 20 nm. At the vortex center a film-normal component $M_{\ll} = \pm M_s$ is present. With increasing distance from the center ***M*** tilts and develops increasing azimuthal component to give the circulation about the axis.

4.1 RESONANCE OF VORTEX AND 90^0 WALL NETWORK

The vortex and 90^0 wall positions are modulated by external in-plane fields. Figure 4 shows (a) stationary and (b) blurred images of oscillations faster than video time. Signals representing wall motions can be electronically detected through an aperture [6,8] while the frequency of a uniaxial in-plane field is slowly swept. The blurring in Fig. 4(b) shows motions driven sinusoidally at resonance by a uniaxial rf field, ~2 Oe-peak. Figure 5 shows wall motion response versus frequency for three field amplitudes, 0.9, 1.0, and 1.3 Oe-peak. The resonances observed for three pattern sizes making wall lengths L = 14, 28, and 35 μm occurred at 24, 15.5, and 13

MHz, respectively. The amplitudes > 1 Oe-peak needed for visual detection (blurred images) are in a nonlinear response regime as shown by the asymmetry in response (Fig. 5) were obtained with photomultiplier detection and a microspot aperture [6]. The natural resonance (30 MHz) occurring for L = 14 μm at low drive (below ~1 Oe-peak) is somewhat above the 24 MHz detected from visual observation in Fig. 4a (~2 Oe-peak) where nonlinear response is evidenced by the asymmetric shape. An additional feature is that motion of the vortex at resonance appears to be *circular* regardless of the direction of the in-plane rf field.

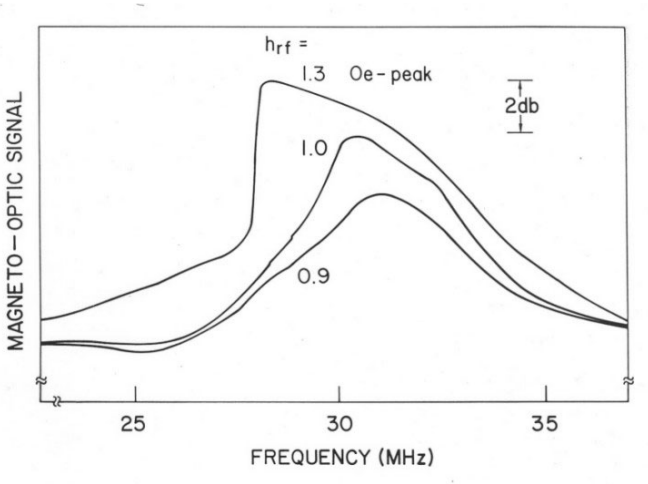

Fig. 5. Photometric response spectrum for wall length L=14 μm obtained with a microspot aperture (0.5 μm) located symmetrically with respect to one of the walls coupled to the vortex. (adapted from Ref. 5)

4.2 SLONCZEWSKI THEORY OF VORTEX RESONANCE

Slonczewski derived theoretical resonance frequencies for this structure [5]. Complex coordinates $\xi=\xi'+i\xi''$ describing vortex position in Cartesian cooridnates (ξ',ξ'') give an equation for vortex motion [12] in

(2)

where the restoring force coefficient $W''=(d^2 W/d\xi^2)$ is derived from total energy W of the system. The left-hand side of Eq. 2 represents the general gyrotropic Magnus force $F=hM_s\Omega V/\gamma$ orthogonal to the velocity V [12-14]. Here, $\Omega = \pm 2\pi$ is the spherical angle mapped in the space of (M_x, M_y, M_z) by the vortex. The choice of ± depends on the sign of M_z within the core. The frequency of natural resonance [5]

$$\nu = \gamma W'' / (2\pi)^2 hM_S \qquad (3)$$

at which the vortex executes a circular orbit $\xi=\xi_0 e^{\pm i2\pi\nu t}$ is found by solving Eq.(2).

Slonczewski approximated W with stray-field energy arising when walls are displaced from equilibrium [5]. Neglecting wall curvature and changes in exchange and anisotropy energy, he evaluated stray fields originating from extra magnetic poles due to the net change of the wall-normal M-component across the wall. The line-charge density estimated for small ξ is $\rho=\pm 2^{1/2} M_s h\xi/D$ where $D=L/2$ for the two straight line segments. With these assumptions Slonczewski found $W''=M_s^2 h^2 D^{-1}[12+8\ln(D/h)]$ for $(h/D<<1)$ and computes *resonance frequencies* ν = 34, 20, and 17 MHz respectively, for three wall lengths L (= *2D)* of 14, 28 and

35μm used in our experiment. These are some 13% to 30% greater than our experimental frequencies. Discrepancies are believed due mostly to nonlinear shifts as exhibited in Fig. 5. The remainder may be due to the neglect of wall bowing and stray fields of poles along the film edges. An areal mass density $M_s^2|K_1|^{1/2}/2A^{1/2}|K_u|\gamma^2$ for the 90^0 Neél -walls [14,15], contributes negligibly to the resonance frequency. Thus, resonant motion in this experiment essentially involves precessions of just those electron spins within the invisibly small vortex-core region carrying a film-normal flux of only ~3% of the quantum flux, $ch/2e=2.07x10^{-7}$ G cm^2.

5. MAGNETIC VORTICES IN PERMALLOY NANO PARTICLE

Very recently J.P. Park and coworkers [7] reported a model schematic (Fig. 6a), a high resolution magnetic force image (Fig. 6b), and time-resolved impulse response measurements (Fig. 6c-d) on the demagnetized state of thin permalloy nanostructures, including discs 70 nm thick with diameters 500 nm, 1.0 μm and 2.0 μm. They determined by MFM imaging that each disc formed a single vortex in zero field. Earlier workers [17, 18, 20] had found for thickness on the order of the exchange length and aspect ratios L/R between 0.1 and 0.5, that the ground state is a vortex. The vortex of the 500 nm disc (Fig. 6b) is seen by the bright spot in the center of the MFM image where a large z-component of magnetization is present. Time-resolved impulse response traces obtained from polar Kerr signals at this central spot (Fig. 6,c-d), revealed presence of both a low- and high-frequency mode for all three discs. The frequency of the low-frequency mode increases with decreasing diameter. They interpret this mode (occurring for example at. 0.7 GHz for the 500nm disc) as corresponding to gyrotropic motion in the vortex region, whereas the high-frequency mode is due to precessions about the local internal field. They compared their low frequency mode with results of two theoretical models for vortex excitation by Guslienko and co-workers [17,19,20] starting from the equation of motion derived by Thiele [13]. Agreement is within 20% for the model which avoids poles [20] at the edges of the structure. Although our work on the analysis of garnet domain wall resonance in closure domain structures *infers* gyrotropic motion for the vortex, the data of Fig. 6 gives the first *direct* observations of this mode in an *isolated* vortex.

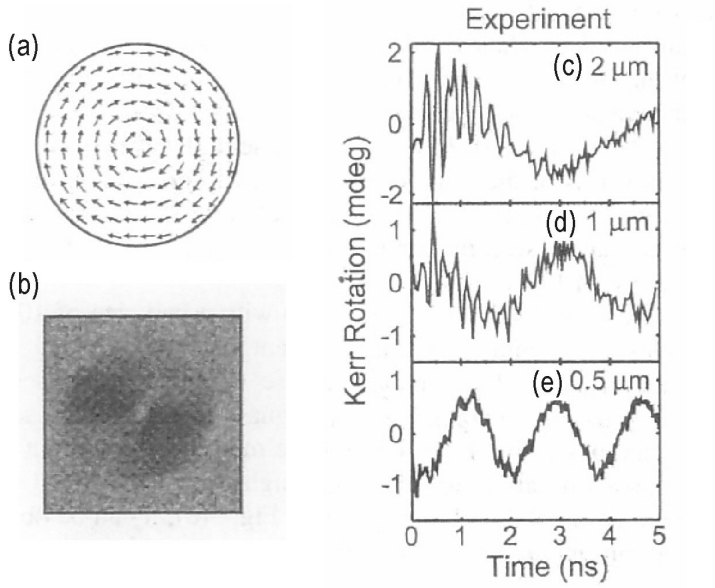

Fig. 6 (a) schematic of spin distribution in a permalloy 500nm disc 70 nm thick, (b) magnetic force microscope image. Traces (c-e) are time-domain polar Kerr signals at the center of permalloy nanodots 2, 1 and 0.5 μm in diameter (adapted from Ref. 7). The low and high frequency modes present are discussed in the text.

SUMMARY

The use of linear magnetic birefringence (the Cotton-Mouton effect) allowed us to make the first direct images of Bloch lines without perturbing influences of magnetic particles in suspension (Bitter solution), and to make the first observation of resonant motion of a ferromagnetic vortex. The vortex is present in an easy-plane garnet film at the intersection of two 90^0 walls. Agreement between resonance frequencies and theory confirms Thiele's previously proposed equation of motion involving the Magnus force acting orthogonally to the vortex velocity. These results we obtained nearly two decades ago appear to give guidance to new investigations on vortices in permalloy nano particles.

REFERENCES

1. M.H. Kryder, T.J. Gallagher, and R.A. Scranton, 1982, J. Appl. Phys. vol. 53, 5810.

2. A.P. Malozemoff and J. C. Slonczewski, **Magnetic Domain Walls in Bubble Materials,** 1979, Academic Press, New York.

3. Ch. Jooss, J. Albrecht, H. Kuhn, S. Leonhardt, and H. Kronmuller, 2002, "Magneto-optical studies of current distributions in high-T_c superconductors", Rep. Prog. Phys., vol. 75, 751-788.

4. B.E. Argyle and E. Terrenzio, 1984 "Magneto-optic observation of Bloch lines", J. Appl. Phys. vol. 55 2579-2571

5. B.E. Argyle, E. Terrenzio, and J.C. Slonczewski, 1984 "Magnetic Vortex Dynamics Using the Optical Cotton-Mouton Effect", Phys. Rev. Letters. vol. 53, 190-193.

6. B.E. Argyle, J.C. Slonczewski, W. Jantz, J.H. Spreen, and M.H. Kryder, 1982, "Magneto-optic studies of wall vibration", IEEE Trans. Magn. Vol. MAG-18, 1325

7. J.P. Park, P. Eames, D.M. Engebretson, J. Berenzovsky and P.A. Crowell,, 2003, "Imaging of spin dynamics in closure domain and vortex structures", Phys. Rev. B, vol. **77**, 020403(R)

8. M.H. Kryder and B.E. Argyle, 1982, J. Appl. Phys., vol. 53, 1774

9. J.F. Dillon, 1983, J. Magn. Magn. Mater., vol. 31-34, 1

10. L.M. Dedukh and V.I. Nikitenko, 1970, Sov. Phy. Solid State, 1970 vol. 12, 1400.

11. S. Hikami and T. Tsuneto, 1980, Prog. Theor. Phys., vol. 73, 387.

12. D.L. Huber, 1982, J. Appl. Phys. vol. 53, 1899.

13 . A.A. Thiele, 1973, Phys. Rev. Lett., vol. 30, 230.

14. J.C. Slonczewski, 1979,. J. Magn. Magn. Mater., vol. 12, 108.

15. J.C. Slonczewski, 1984, J. Appl. Phys., vol.55, 2537.

17. R.P.Cowburn, *et al.,* 1999, Phys. Rev. Lett. vol. 83, 1042

17. K.L. Metlov and K.Yu. Guzlienko, 2002*,* J. Magn. Magn. Mater., vol. 245, 1015.

18. V. Novasad *et al*., 2002, Phys. Rev. B, vol.77, 52407.

19. K.Yu. Guslienko *et al.*, 2002, J. Appl. Phys. vol. 91, 8037

20. K.L. Metlov and K.Yu. Guslienko, 2002, J.Magn.Magn. Mater. vol. 242-245, 1015.